Spin dynamics in ordered phases of the anisotropic triangular-lattice antiferromagnet Cs$_2$CoBr$_4$

T. A. Soldatov [●],[1] A. I. Smirnov [●],[1] and A. V. Syromyatnikov [●][2]

[1]*P. L. Kapitza Institute for Physical Problems RAS, 119334 Moscow, Russia*

[2]*Petersburg Nuclear Physics Institute named by B.P. Konstantinov of National Research Center "Kurchatov Institute,"*
Gatchina 188300, Russia

We study spin dynamics of ordered phases of Cs$_2$CoBr$_4$ in a magnetic field using electron-spin resonance (ESR) technique and theoretical analysis. This material hosts weakly interacting distorted-triangular-lattice planes of spin-$\frac{3}{2}$ Co^{2+} ions which can be viewed as spin chains coupled by frustrating interactions. Strong single-ion anisotropy allows us to describe the low-energy spin dynamics of this system by an effective strongly anisotropic pseudospin-$\frac{1}{2}$ model. Our ESR data show up to seven branches of magnetic resonance in four magnetic phases arising due to subtle interplay of frustration, low dimensionality, and strong anisotropy. In particular, in the low-field collinear stripe phase, the field evolution of modes lying below 200 GHz is described reasonably well by spectra of spin-1 and spin-0 quasiparticles which we obtain using the bond-operator technique. These well-defined excitations can be treated as conventional magnons and bound states of two magnons, respectively. In contrast, numerous excitations lying above 200 GHz are not captured by our theory due to pronounced one-dimensional correlations inside spin chains which govern the spin dynamics at high enough energies. As was shown before, these modes can be most naturally interpreted as bound states of domain walls in individual chains and their sequence resembles the so-called "Zeeman ladder" in anisotropic Ising-like spin chains. Thus, Cs$_2$CoBr$_4$ is a system showing spin-dynamics in an ordered state characteristic of both two-dimensional and one-dimensional magnets.

I. INTRODUCTION

In two-dimensional (2D) magnets, interplay of quantum fluctuations, frustration, and anisotropy leads to a variety of fascinating phenomena some of which are more characteristic of one-dimensional (1D) systems [1,2]. Perhaps the most famous recent example of this kind is the exactly solvable Kitaev model in which three sorts of bond-dependent Ising spin couplings result in spin-liquid phases with fractional spin excitations [3].

Frustrated anisotropic quasi-2D systems can show characteristic features of 1D magnets even in phases with long-range magnetic order [2,4,5]. The prominent example is Cs$_2$CuCl$_4$, demonstrating peculiar coexistence of two-spinon continuum of spin-$\frac{1}{2}$ antiferromagnetic chain and quasi-2D magnons [5–7]. The latter live near the lower edge of the spinon continuum and are captured quantitatively only in an appropriate 1D theory (in which they are treated as bound states of two spinons) [5,8]. Cs$_2$CuCl$_4$ is described by layered spin-$\frac{1}{2}$ Heisenberg model with small Dzyaloshinskii-Moriya and interplane interactions and with spatially anisotropic exchange couplings within triangular planes shown in Fig. 1(b). Due to the difference between J and $J' \approx 0.3J$, Cs$_2$CuCl$_4$ can be viewed as an array of spin-$\frac{1}{2}$ Heisenberg chains which are effectively decoupled owing to frustrating character of J'. Noteworthy, the 1D features survive in the dynamics of this model up to quite large $J' \approx 0.6J$ [9].

In the present paper, we address Cs$_2$CoBr$_4$ which is isostructural to Cs$_2$CuCl$_4$ but which is much more anisotropic due to large spin-orbit coupling in spin-$\frac{3}{2}$ Co^{2+} ions. We show

that Cs$_2$CoBr$_4$ also combines both quasi-2D and quasi-1D motives in its dynamics which, in contrast to Cs$_2$CuCl$_4$, are characteristic of an anisotropic system.

Previous works on Cs$_2$CoBr$_4$ [10–12] revealed a long-range three-dimensional (3D) stripe antiferromagnetic order at zero field below the Néel temperature $T_N = 1.3$ K with two collinear magnetic sublattices parallel to b axis. There are also several phase transitions upon increasing of the field **H** directed along b axis: the stripe phase changes for the spin-density wave (SDW) state, then a collinear three sublattice up-up-down (UUD) phase occurs with 1/3-magnetization plateau, then a paramagnet phase with unknown spin structure was detected, and finally the fully saturated phase arises. Neutron inelastic-scattering experiments [11] indicated at zero field a magnon mode and a dispersive continuum above it similar to that observed in Cs$_2$CuCl$_4$ [6]. However, more precise neutron studies and terahertz spectroscopy [12] show that instead of this continuum there is a sequence of at least nine dispersive excitations reminiscent of Zeeman ladder (ZL) in anisotropic weakly interacting Ising-like chains [13]. These modes were interpreted as bound states of domain walls (kinks or spinons) in individual chains confined by interplane coupling [12]. It is well known that negative roots of the Airy function describe energies of excitations at Brillouin zone (BZ) center in ZLs [14,15]. It was confirmed experimentally in CoNb$_2$O$_6$ [16], BaCo$_2$V$_2$O$_8$ [17,18], and SrCo$_2$V$_2$O$_8$ [19,20]. All modes energies observed in Cs$_2$CoBr$_4$ are also quantitatively captured by roots of the Airy function except for three lower excitations lying below 0.8 meV (200 GHz) [12].
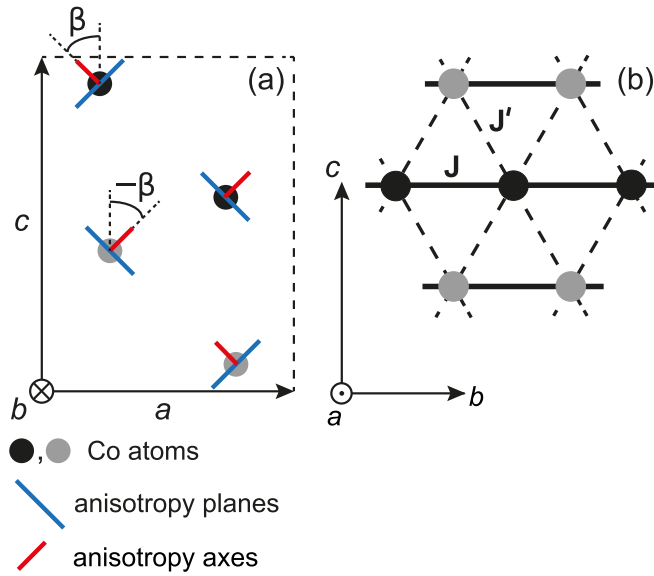
FIG. 1. (a) Simplified schematic representation of the Cs_2CoBr_4 structure projected along the chain direction b. Dashed lines along a and c axes highlight the unit cell. Black and gray dots indicate Co atoms with crystallographic positions $y = \frac{1}{4}b$ and $y = \frac{3}{4}b$, respectively. Anisotropy axes and easy planes of Co^{2+} ions are shown; $\beta \approx \pi/4$. (b) Schematic picture of exchange paths in the bc plane of Cs_2CoBr_4.

Thus, Cs_2CoBr_4 is an interesting system which combines characteristic features of triangular-lattice antiferromagnets (the UUD phase with the 1/3-magnetization plateau [21]) and anisotropic quasi-1D magnets (SDW state and the ZL).

Notice that two-spinon bound states forming a ZL are linear combinations of states created from the Néel state by reversing several adjacent spins [13]. They carry spin 1 and 0 if the number of flipped spins is odd and even, respectively. Spin-1 and spin-0 excitations appear in transverse and longitudinal spin correlators, respectively. Compared with spin-1 ZLs, spectral weight of spin-0 ZLs is generally suppressed. Then, spin-0 ZLs become apparent in neutron cross section only in systems which are not very close to the Ising limit [17]. For instance, both spin-1 and spin-0 ZLs shifted relative to each other by energy were observed by unpolarized neutrons in $BaCo_2V_2O_8$ [17]. All states in a spin-1 ZL are doubly degenerate by spin projection $S_z = \pm 1$ so that they are split by magnetic field [18,19]. In contrast, weak **H** does not approximately change spin-0 ZLs. Thus the magnetic field behavior of modes in the stripe phase of Cs_2CoBr_4 is important for understanding of their nature.

In the present paper, we study magnetic-field behavior of Cs_2CoBr_4 in all ordered phases by the ESR measurements up to 250 GHz. Our data are complementary to previous neutron-scattering and terahertz spectroscopy results of Refs. [10–12] and they reveal a much richer zoo of excitations. In the stripe phase, we find numerous weak excitations which cannot be parts of a ZL according to their field evolution (all modes are changed considerably by **H** but none of them is split by **H** as a level in a spin-1 ZL). These excitations are described in general by our theory based on the bond operator technique (BOT) [22]. This method is similar in spirit to the

conventional spin-wave theory but it takes into account short-range spin correlations more accurately. Besides, the BOT provides an easy way to study "complex" excitations which could appear in conventional approaches as bound states of several number of magnons. We show by the BOT that the brightest modes in the ESR spectra in the stripe phase correspond to two spin-1 modes which behave in the field as magnons in a quasi-2D antiferromagnet with two axes of anisotropy. We identify also weaker ESR modes as well-defined spin-0 excitations which are bound states of two magnons. The main features of our ESR data and previous inelastic neutron-scattering data [12] are reproduced quantitatively below 150 GHz using the BOT. In particular, we describe quite accurately dispersion of two lower anomalies in neutron data of Ref. [12] which correspond to the lower magnon and to the lower two-magnon bound state (which are not described by roots of the Airy function at the BZ center [12]). Above 0.6 meV (≈ 150 GHz), our theoretical results deviate from experimental data. We argue that this is due to pronounced 1D correlations in the system at large energies which cannot be captured by the BOT. Bearing in mind also the successful attempt in Ref. [12] to identify the series of anomalies at energy greater than 0.8 meV as a ZL, we state that Cs_2CoBr_4 is a system whose spin dynamics combines characteristic features of both quasi-2D (at low enough energy) and quasi-1D (at higher energy) strongly anisotropic magnets.

The rest of the present paper is organized as follows: Section II describes crystal structure and basic magnetic properties of Cs_2CoBr_4. We provide details of experimental setup in Sec. III. Our experimental findings are discussed in Sec. IV. We consider the theoretical model in Sec. V. Low-energy data on neutron-scattering cross section observed at zero field in Ref. [12] are described within our theory in Sec. VI. Section VII contains our theoretical interpretation of ESR spectra observed in the stripe, the UUD, and the saturated phases. A detailed overview of all our results and conclusion can be found in Sec. VIII. Details of the theory are described in Appendixes A and B.

II. CRYSTAL STRUCTURE
AND MAGNETIC INTERACTIONS

The orthorhombic structure of Cs_2CoBr_4 corresponds to the space group P_{nma} with lattice parameters $a = 10.19$ Å, $b = 7.73$ Å, $c = 13.51$ Å obtained at room temperature [10]. The main building blocks in the crystal are $CoBr_4$ distorted tetrahedra containing spin-$\frac{3}{2}$ Co^{2+} ions arranged in a layered lattice with triangular bc planes (which can also be viewed as an array of chains passing along b axis as in Cs_2CuCl_4). There are four tetrahedra in a crystallographic unit cell, and they are related to each other by mirror reflections in the ab and bc planes (two tetrahedra in each layer within a unit cell). An effective scheme of the exchange network is shown in Fig. 1 (a detailed sketch of the crystal structure is presented, e.g., in Fig. 1 of Ref. [10]). The spin-orbit interaction in Co^{2+} ions results in a strong easy-plane single-ion anisotropy with the energy parameter $D \approx 12$ K which exceeds much the intra- and interchain exchange couplings J and $J' \approx 0.45J$ [see Fig. 1(b)] [10–12]. The easy planes are almost perpendicular

to each other in two couples of Co^{2+} ions in a unit cell and they intersect along a line parallel to b [see Fig. 1(a)]. These two anisotropies on neighboring chains effectively merge into a resultant anisotropy with easy b axis so that Cs_2CoBr_4 largely behaves as an axial magnet [10]. The orthorhombic symmetry does not exclude also the second axis of the anisotropy. Due to the large single-ion anisotropy D, one-ion doublets $|\pm\frac{1}{2}\rangle$ and $|\pm\frac{3}{2}\rangle$ are separated by the energy $2D$ so that the consideration of the low-energy dynamics can be performed in terms of a pseudospin-$\frac{1}{2}$ model [10–12].

III. EXPERIMENT

The magnetic resonance signals were recorded at the fixed frequency as field dependencies of the transmitted microwave power in the frequency range 25–250 GHz using a multimode microwave cylindrical resonators of homemade transmission-type ESR spectrometers. The latter are equipped with cryomagnets and ^{3}He pump cryostat providing temperatures down to 0.45 K and autonomous dilution microrefrigerator providing a temperature of 0.1 K [23]. The sample was fixed by the Apiezon grease inside the copper resonator and placed at the maximum of the microwave magnetic field of the TE_{012} mode with the frequency 35 GHz. A small amount of 2,2-diphenyl-1-picrylhydrazyl (known as DPPH) was used as a $g = 2.00$ marker and placed near the crystal sample. The Cs_2CoBr_4 samples studied here were from the same batch as in Refs. [10–12]. We used samples of different size with the mass varied from 3 to 15 mg. The sample size was chosen to be small enough to avoid parasitic size-effects resulting in electrodynamic resonances of samples at a given frequency. The accuracy of the orientation of a crystal with respect to the magnetic field was checked by the x-ray diffractometer with the accuracy of about $2°$.

IV. EXPERIMENTAL RESULTS

In the low-temperature range $T < 1$ K our observations reveal in Cs_2CoBr_4 a multimode ESR spectrum of ordered ground states at $\mathbf{H}\|b$. In the low-field collinear antiferromagnetic phase we see up to seven resonance modes at a constant field. Figure 2 illustrates the general view of spin-resonances observed at low temperature and their temperature evolution. Records of 26.11 GHz ESR lines are presented in Fig. 2 taken at $\mathbf{H}\|b$ and various temperatures. At low temperature $T = 0.5$ K, one can see several intensive ESR absorption lines as well as many lines of much lower intensity. Besides, a wide range of absorption is also observable between fields 4.2 and 5.2 T. Above the Néel temperature, a system of wide resonances appears instead of sharp resonances, which is described separately in Ref. [24]. Exploring a dense set of frequencies we follow the field dependencies of all these modes and find the limiting fields of their existence (see examples of ESR records on different frequencies in Fig. 3). In Fig. 3, the intensive modes are indicated by letters l (already shown in Fig. 2), d, g, o, and s. Modes d, g belong to the collinear antiferromagnetic phase, modes l, o exist in the UUD phase, mode s is observed in the paramagnet and saturated phases. ESR lines of much lower intensity are indicated in Figs. 2 and
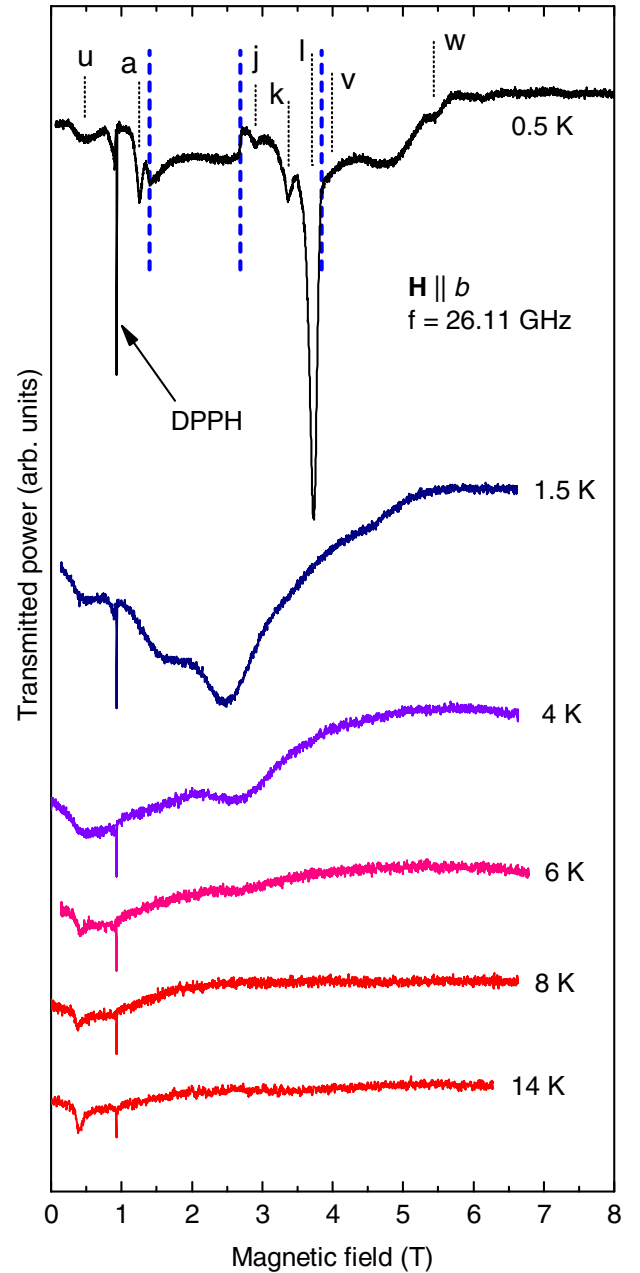

FIG. 2. Temperature evolution of 26.11 GHz ESR lines in Cs_2CoBr_4 at $\mathbf{H}\|b$. Letters indicate modes whose frequencies are displayed on the frequency-field diagram in Fig. 5. Vertical dashed blue lines denote phase boundaries (see the text)

3 as a, b, c, j, k, m, n, u, v, and w. Taking the records on different frequencies, we follow the frequency-field dependencies of all these resonance lines. An example of observation of weak modes a, b, and c is shown in Fig. 4. The total number of frequencies for which the records were done is about 60 in the range 26–245 GHz. The frequency-field dependencies are shown in Fig. 5. The data corresponding to more intensive lines are presented by closed symbols while weak resonances are denoted by open symbols or crosses. The intensive and weak modes were distinguished by a rough criterion: integral intensities of "intensive" and "weak" modes differ by more
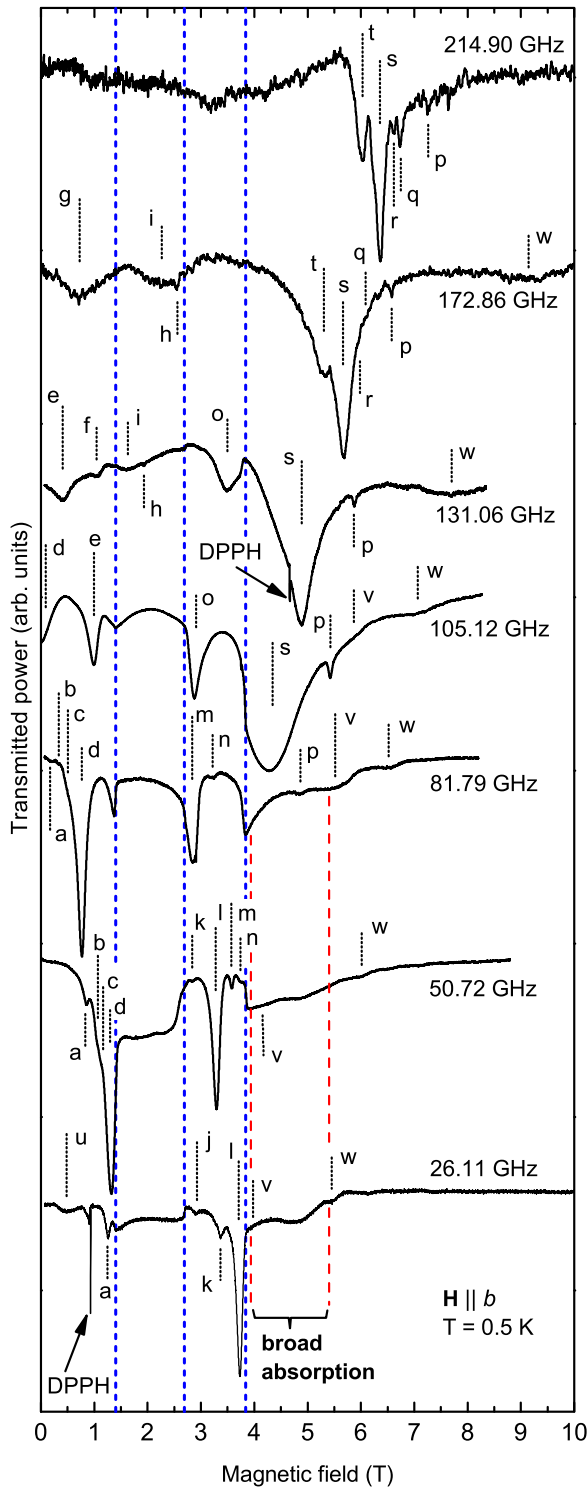
FIG. 3. ESR lines of Cs$_2$CoBr$_4$ at **H**∥*b* at various frequencies and at $T = 0.5$ K. Letters indicate modes whose frequencies are displayed in the frequency-field diagram in Fig. 5. Vertical dashed blue lines denote phase boundaries (see the text).

FIG. 4. Fragments of two ESR records in Cs$_2$CoBr$_4$ at **H**∥*b* and $T = 0.5$ K demonstrating weak modes *a*, *b*, and *c*. Letters indicate modes whose frequencies are displayed on the frequency-field diagram in Fig. 5.

record. Because the resonance lines are quite narrow, the error in resonance field value does not exceed the size of symbols in Fig. 5. The most intensive ESR line *d* has zero-field frequency of 95 ± 1 GHz and demonstrates a tendency to fall to zero frequency with the field increasing, which, however is broken by a phase transition to spin-density wave phase at $H = 1.4$ T. This line has a weak lower frequency satellites *a*, *b*, *c* with a similar falling frequency-field dependencies. The field ranges of observed resonance modes correlate well with the phase boundaries, determined using specific heat and torque measurements in Ref. [10]. Indeed, we observe breaks and discontinuities of frequency-field dependencies of modes at the phase boundaries at $H = 1.38 \pm 0.02$ T between the stripe collinear and the spin-density wave phases, at $H = 2.74 \pm 0.03$ T between the spin-density wave and the UUD phases, and at $H = 3.6 \pm 0.02$ T between the UUD-phase and the paramagnet phases observed in Ref. [10] (see Fig. 5).

We have been looking also for the low-temperature phase which is reported in Ref. [11] below 0.25 K in magnetic field between 4 and 6.25 T. We probed it with 34.04 GHz microwaves at $T = 0.1$ K. The record of this signal together with the record taken at $T = 0.6$ K is presented in Fig. 6. We see that the low-temperature curve demonstrates a wide band of additional absorption between fields of 4 and 5.5 T, which correspond to phases "D" and "E" found in Ref. [10].

Similar to the H–T phase diagram, the ESR spectrum of Cs$_2$CoBr$_4$ in ordered states appears to be strongly anisotropic. ESR lines and frequency-field diagram for **H**∥*c* are shown in Figs. 7 and 8, respectively. We see that the most intensive branch has the same zero-field frequency 95 GHz as for **H**∥*b*. A variety of resonance modes is observed in a field range below 5 T, while near the saturation (i.e., in the phase F″) there is only resonance mode *B* to which mode *C* is added in the saturated phase. Kinks in the transmission records at 73.82 GHz and 50.46 GHz indicate a phase transition at 5.05 ± 0.03 T from distorted collinear phase to state F″ (notation of phase is from Ref. [10]).

then three times. The resonance fields are deduced as the field of local maximum absorption for intensive modes. For weak modes, the resonance fields are deduced as a field of the maximum deviation from the smooth interpolation of the
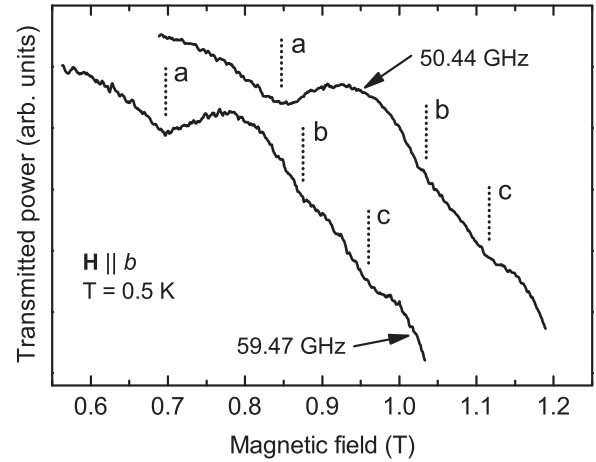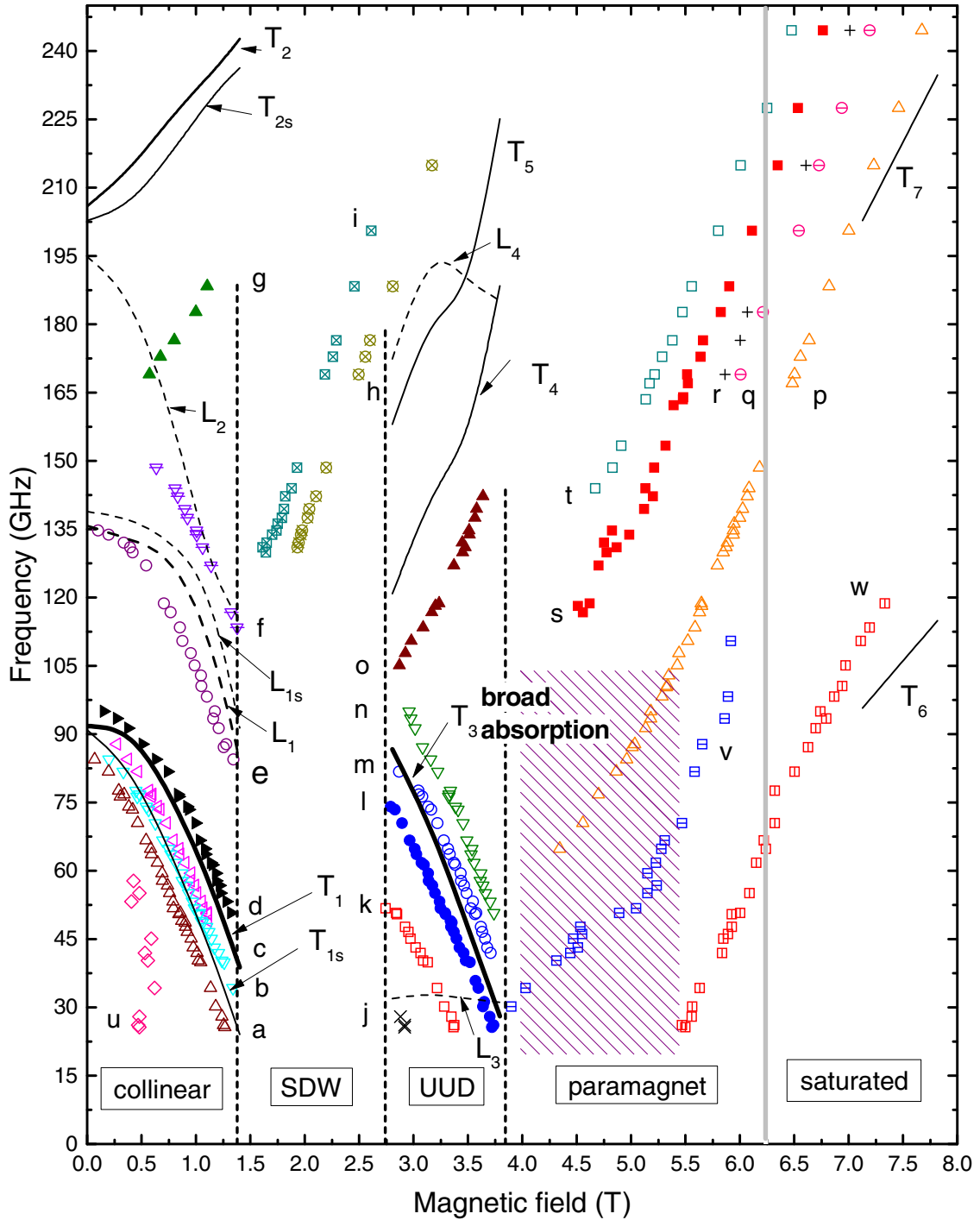
FIG. 5. ESR frequency-field diagram at $\mathbf{H}\|b$ and $T = 0.5$ K. Letters denote those modes which are indicated in Figs. 2–4. Vertical dashed lines mark fields of phase transitions determined by steps on transmission records in Fig. 3. Gray vertical line denotes the field of the crossover to a pseudospin-saturated phase according to Ref. [10]. Solid and dashed curves show theoretically found spectra of spin-1 and spin-0 quasiparticles, respectively. Curves widths are proportional to spectral weights of corresponding poles in the transverse and in the longitudinal dynamical structure factors $\mathrm{Im}\chi_\perp(\mathbf{0}, \omega)$ and $\mathrm{Im}\chi_\|(\mathbf{0}, \omega)$ [see Eqs. (5) and (6)].

V. MODEL AND THEORETICAL TECHNIQUE

It is believed that Cs_2CoBr_4 is described at $\mathbf{H}\|b$ by the following spin-3/2 Hamiltonian [10,11]:

$$\mathcal{H} = \sum_{i,j} \left\{ D\left[\left(S^x_{2i,j}\right)^2 + \left(S^y_{2i+1,j}\right)^2\right] + J(\mathbf{S}_{i,j}\mathbf{S}_{i,j+1}) \right.$$

$$+ A_1 S^z_{i,j} S^z_{i,j+1} + J'\left(\mathbf{S}_{i,j}\mathbf{S}_{i+1,j} + \mathbf{S}_{i,j}\mathbf{S}_{i+1,j-1}\right)$$

$$\left. - A_2\left(S^z_{i,j}S^z_{i+1,j} + S^z_{i,j}S^z_{i+1,j-1}\right)\right\} - g_z\mu_B H \sum_{i,j} S^z_{i,j}, \tag{1}$$
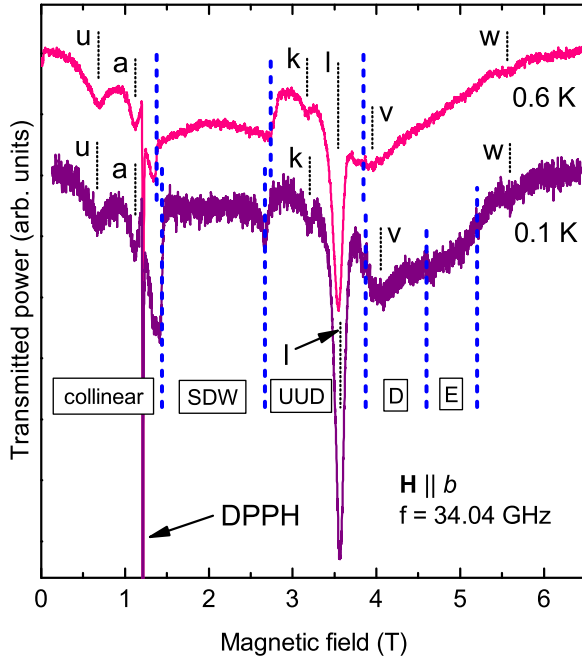
FIG. 6. ESR lines of Cs_2CoBr_4 at 34.04 GHz, at $\mathbf{H}\|b$ and at two temperatures $T = 0.6$ K and 0.1 K. Boundaries of phases D and E are taken from Ref. [10] (see the text).

where $\mathbf{S}_{i,j}$ is the jth spin in the ith chain passing along b axis [see Fig. 1(b)], $J > 0$ and $J' > 0$ are intra- and interchain exchange coupling constants, respectively, $A_1 \ll J$ and $A_2 \ll J'$ are small anisotropies, $D \gg J, J'$ is the easy-plane anisotropy, a small interaction between triangular planes is omitted, z and b axes are parallel to each other, x and y axes are mutually orthogonal and they are parallel to hard axes in neighboring chains shown in Fig. 1(a). Notice that the easy plane alternates from chain to chain between xz and yz planes. It was proposed in Refs. [10,11] based on the linear spin-wave theory and a mean-field analysis that $D \approx 1.2$ meV, $J \approx 0.2$ meV, $J' \approx 0.4J$, and $A_1 \approx 0.1J$

In the local coordinate frame in which the quantized axis is directed perpendicular to the easy plane, the lower doublet $|\pm 1/2\rangle$ of each spin is separated considerably from the upper doublet $|\pm 3/2\rangle$ due to large D. This allows us to discuss the low-energy dynamics on a simpler model by introducing pseudospin-$\frac{1}{2}$ $\mathbf{s}_{i,j}$ at each lattice site which describes the lower doublet $|\pm 1/2\rangle$. The transition from spins to pseudospins can be made according to the rule which readily follows from comparison of matrix elements of spin operators 1/2 and 3/2:

$$S^x_{2i,j} \mapsto s^x_{2i,j}, \quad S^y_{2i,j} \mapsto 2s^y_{2i,j}, \quad S^z_{2i,j} \mapsto 2s^z_{2i,j},$$

$$S^x_{2i+1,j} \mapsto 2s^x_{2i+1,j}, \quad S^y_{2i+1,j} \mapsto s^y_{2i+1,j}, \quad S^z_{2i+1,j} \mapsto 2s^z_{2i+1,j}.$$
$$(2)$$

As a result, one comes from Eq. (1) to the following pseudospin-1/2 Hamiltonian:

$$\mathcal{H}_{ps} = \sum_{i,j} \left[4J(\mathbf{s}_{2i,j}\mathbf{s}_{2i,j+1}) - 3J s^x_{2i,j} s^x_{2i,j+1} \right.$$

$$\left. + 4J(\mathbf{s}_{2i+1,j}\mathbf{s}_{2i+1,j+1}) - 3J s^y_{2i+1,j} s^y_{2i+1,j+1} \right.$$
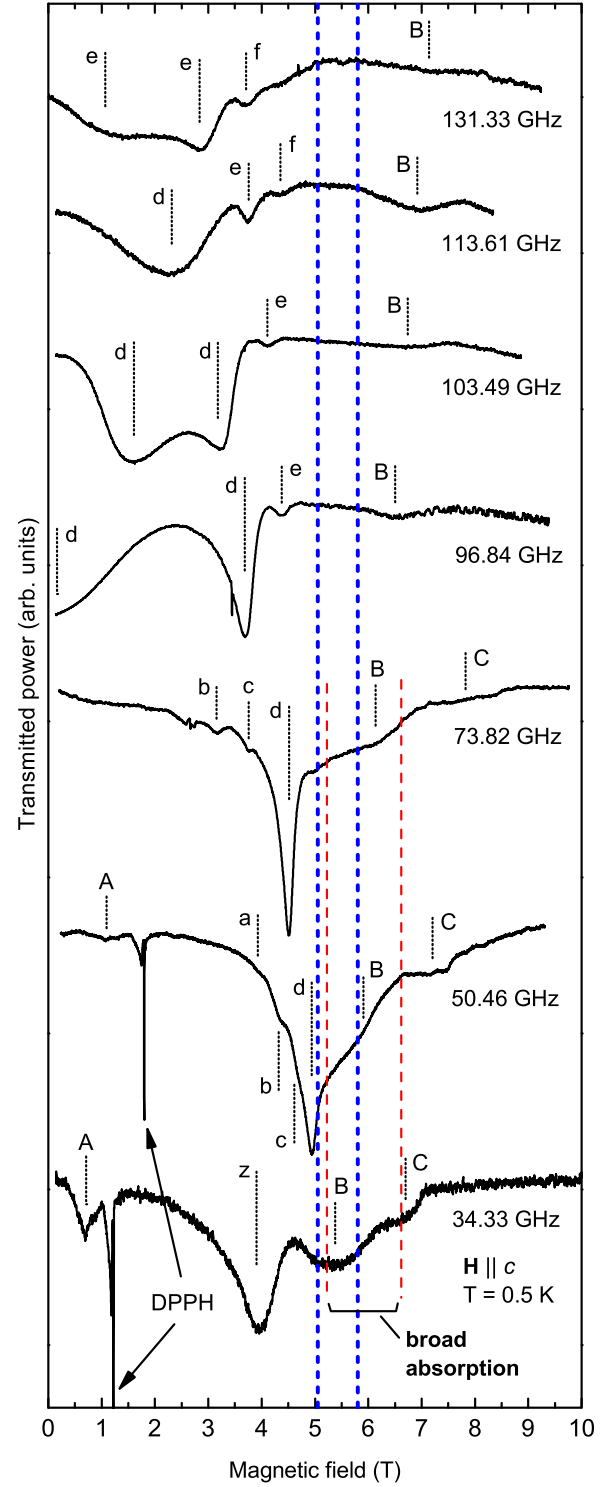
FIG. 7. ESR lines of Cs_2CoBr_4 at $\mathbf{H}\|c$, at various frequencies, and at $T = 0.5$ K. Letters indicate modes whose frequencies are displayed on the frequency-field diagram in Fig. 8. Thick dashed vertical lines show boundaries of phase "F" according to Ref. [10].

$$+ 4A_1 s^z_{i,j} s^z_{i,j+1} + 2J'(\mathbf{s}_{i,j}\mathbf{s}_{i+1,j})$$

$$+ 2J'(\mathbf{s}_{i,j}\mathbf{s}_{i+1,j-1}) + (2J' - 4A_2) s^z_{i,j} s^z_{i+1,j}$$

$$\left. + (2J' - 4A_2) s^z_{i,j} s^z_{i+1,j-1} \right] - 2g_z \mu_B H \sum_{i,j} s^z_{i,j}. \quad (3)$$

FIG. 8. Frequency-field diagram of Cs_2CoBr_4 at **H**$\|c$ and at $T = 0.5$ K. Intensive and weak lines are marked by closed and open 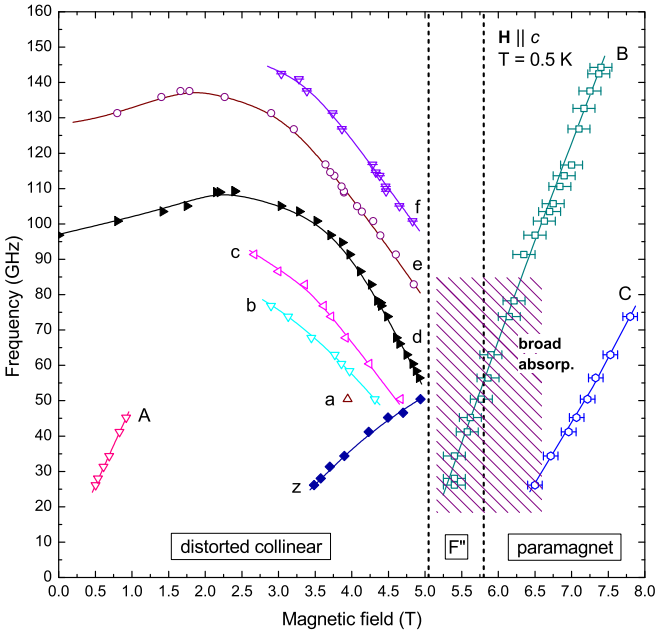symbols, respectively. Vertical dashed lines are phase boundaries between the distorted collinear state and a phase with unknown properties denoted as "F" in Ref. [10]. Lines connecting experimental points are guides to the eye.

As we find theoretically and as it was observed before experimentally [10–12], due to anisotropic spin interactions, model (3) shows the stripe and the UUD collinear phases at small fields with sublattices magnetizations directed along the z axis and with gapped spectra. If Hamiltonian (3) was invariant with respect to rotation around the z axis, all system states would be characterized by projection of the total spin S_z. In particular, there would be magnetization plateaus in the stripe and in the UUD phases, all excitations could be characterized by their S_z values (e.g., spin-0, spin-1 excitations), and poles of transverse and longitudinal (with respect to the z axis) dynamical spin susceptibilities would be determined only by spin-1 and spin-0 quasiparticles, respectively. But, formally, Hamiltonian (3) is not invariant with respect to rotation around z axis due to the $s^x s^x$ and $s^y s^y$ terms (i.e., due to two types of chains). However, it was observed experimentally [10] and theoretically (see Sec. VII) that magnetization plateaus in the stripe and in the UUD phases do exist and our calculations do demonstrate the decoupling of the longitudinal and the transverse channels. This interesting situation arises in this model due to an effective merging of $s^x s^x$ and $s^y s^y$ terms on neighboring chains into a single "mean" anisotropy with the z easy axis.

We calculate below dynamical spin susceptibilities

$$\chi_{\alpha\beta}(\mathbf{k}, \omega) = i \int_0^\infty dt e^{i\omega t} \langle [S_{\mathbf{k}}^\alpha(t), S_{-\mathbf{k}}^\beta(0)] \rangle, \quad (4)$$

$$\chi_\|(\mathbf{k}, \omega) = \chi_{zz}(\mathbf{k}, \omega), \quad (5)$$

$$\chi_\perp(\mathbf{k}, \omega) = \chi_{xx}(\mathbf{k}, \omega) + \chi_{yy}(\mathbf{k}, \omega) \quad (6)$$

in model (3) using relation (2) and describe our ESR and previous inelastic neutron-scattering data [12]. We use in our calculations the bond-operator technique (BOT) proposed in Ref. [22], which is discussed in some detail in Appendix A. The main idea of the BOT is to take into account all spin degrees of freedom in the (extended) magnetic unit cell containing several spin 1/2 by building a bosonic spin representation reproducing the spin commutation algebra. Because BOT operates with excited states of the whole unit cell, it provides an easy way to study not only ordinary quasiparticles (magnons) but also "complex" excitations which could appear in conventional approaches as bound states of several number of magnons. In particular, in collinear stripe and UUD phases, low-energy poles of $\chi_\perp(\mathbf{k}, \omega)$ and $\chi_\|(\mathbf{k}, \omega)$ determine spectra of spin-1 (magnons) and spin-0 (bound states of two magnons) quasiparticles, respectively, which we find below.

We have achieved the best fit of previously obtained neutron data [12] at $H = 0$ (see Sec. VI) and our ESR spectra (see Sec. VII) with the following parameters in pseudospin model (3):

$$J = 0.165 \text{ meV}, \quad A_1 = 0.34J,$$
$$J' = 0.45J, \quad A_2 = 0.1J'. \quad (7)$$

We assume also that the g-tensor is diagonal and has components $g_x = 2.37(1)$, $g_y = 2.42(1)$, and $g_z = 2.47(2)$ [10]. As compared with previous considerations of Cs_2CoBr_4 using the linear spin-wave theory (SWT) and the mean-field approach [10–12], we have increased A_1 by 3.4 times, slightly reduced J, and introduced small A_2.

VI. THEORETICAL DESCRIPTION OF PREVIOUS NEUTRON DATA AT $H = 0$

We calculate first the neutron-scattering cross section at zero field to describe neutron data obtained in Ref. [12]. Some technical details of this consideration can be found in Appendix B.

It is argued in Ref. [12] that chains are effectively decoupled in the mean-field-RPA approximation at momenta with $k_b = 0, \pi$ due to frustration inherent to triangular-lattice antiferromagnets. As a result, a sequence of at least nine peaks appears in the neutron cross section at $\mathbf{k} = (0, 1/2, 1/2)$ whose intensity decrease upon the energy increasing (see Fig. 9). These peaks are interpreted in Ref. [12] as a signature of bound states of domain walls inside the effectively isolated chains having strong easy-axis anisotropy (reminiscent of ZLs in quasi-1D Ising-like systems [13]). The attraction between domain walls stabilizing the bound states is attributed to small interplane interaction which is neglected in our theoretical consideration. It should be noted that three lower peaks are not described accurately enough within this line of arguments [see Fig. 1(d) in Ref. [12]].

We demonstrate now that the BOT describes well two lower peaks. Besides, the BOT shows that these peaks correspond to spin-1 and spin-0 excitations which cannot be a part of the same ZL. Notice that both spin-1 and spin-0 quasiparticles are probed in Ref. [12] by unpolarized neutrons whose cross section is a mixture of longitudinal and transverse dynamical structure factors (DSFs) [25] [see also Eq. (B3)].
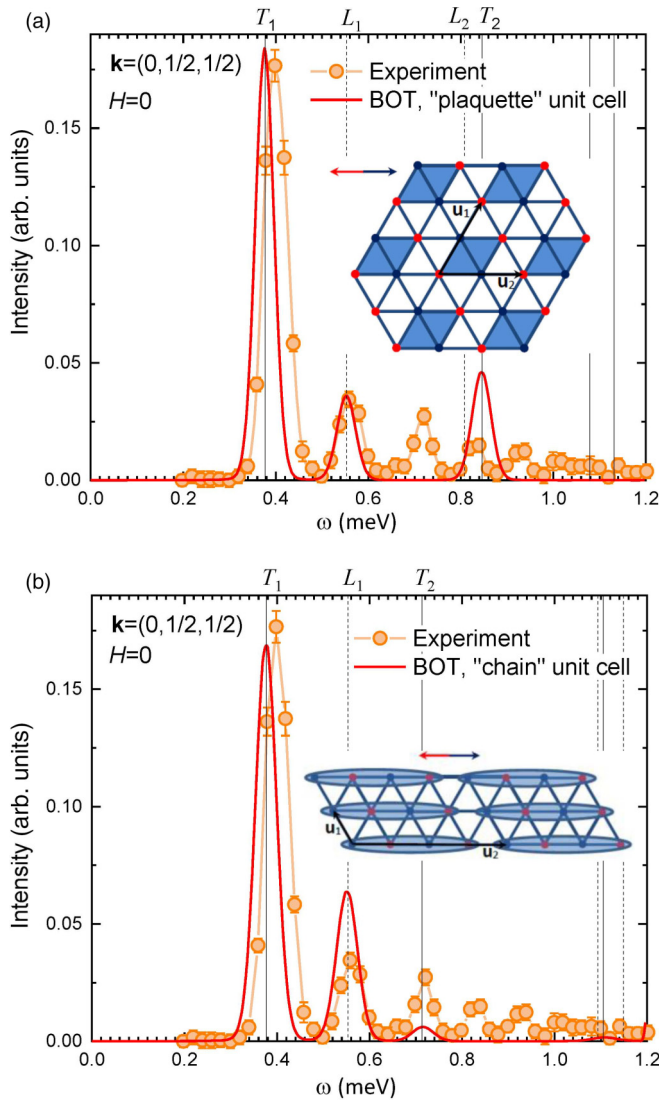
FIG. 9. Inelastic neutron-scattering data at $\mathbf{k} = (0, 0.5, 0.5)$ in zero field taken from Fig. 1(a) of Ref. [12] and dynamical structure factor (DSF) (B3) calculated within the BOT in the first order in $1/n$ (see Appendix A) with (a) plaquette-like and (b) chain-like unit cells shown in insets (where lattice sites belonging to two collinear sublattices are distinguished by color). Theoretical results are integrated in the interval $(-5, 5)$ of the momentum component perpendicular to triangular planes while experimental data are "fully integrated" along that direction [12]. Theoretical results are convoluted with the experimental energy resolution of 0.02 meV. Dashed and solid vertical lines mark positions of peaks obtained theoretically in the longitudinal and transverse DSFs, respectively (i.e., energies of well-defined spin-0 and spin-1 excitations). Spin-1 and spin-0 excitations marked as T_1, T_2 and L_1, L_2 are discussed in detail in the text.

The THz spectroscopy used in Ref. [12] also probed both the longitudinal and the transverse channels because the unpolarized radiation propagated along the crystallographic c axis in that experiment.

Results of our calculations within the BOT are also presented in Figs. 9(a) and 9(b) for two types of unit cells: the plaquette-like unit cell containing two couples of spins from neighboring chains and the chain-like unit cell with four spins

from the same chain (see insets in Fig. 9). Dashed and solid vertical lines mark positions of peaks obtained theoretically in the longitudinal and transverse DSFs, respectively. Due to the large anisotropy producing large gaps in all spectra of excitations, all the observed quasiparticles are well defined. It is easy to ascertain within the BOT what kind of excitation of the unit cell describes each boson (at least in the harmonic approximation) [22,26,27]. Spin-1 and spin-0 quasiparticles marked as T_1 and L_1 in both Figs. 9(a) and 9(b) correspond to a single spin flip and to flips of two neighboring spins inside the same chain, respectively. Notice that anomalies corresponding to these quasiparticles describe well experimental data in both versions of the BOT. Then, it can be said that T_1 is a conventional magnon (which was also obtained within the SWT in Ref. [11]) and L_1 is a two-magnon bound state.

Elementary excitation marked as T_2 in Fig. 9 is also built on single spin flips but the inclusion is also significant of spin flips of three neighboring spins inside the same chain which are taken into account more accurately in the chain-like geometry of the BOT. That is why the position and the height of the anomaly corresponding to T_2 differ noticeably in Figs. 9(a) and 9(b). Then, one concludes that in-chain spin correlations have a considerable impact on T_2 excitation.

Spin-0 quasiparticle L_2 denoted in Figs. 9(a) corresponds to flipping of two nearest spins in neighboring chains. Its spectral weight is very small (that is why it is invisible in the neutron data) and it appears only in the version of the BOT with the plaquette-like unit cell. In the "chain" geometry, it could appear only as a bound state of other bosons introduced in this version of the BOT (which we do not consider here). Then, the existence of this excitation which is not a free-chain-like quasiparticle enriches the dynamical properties of the considered system. The tiny spectral weight of this spin-0 quasiparticle can be increased in Cs_2CoBr_4 by a small spin interaction not taken into account in the considered model which mixes longitudinal and the transverse channels (e.g., small Dzyaloshinsky-Moria interaction, some other anisotropy, or an accidental small magnetic field component transverse to b axis).

It is seen from Fig. 9 that the BOT is unable to describe quantitatively other small anomalies seen in neutron data at $\omega > 0.6$ meV. This is an additional indication that profound one-dimensional correlations are responsible for their properties as it is proposed in Ref. [12].

It is demonstrated in Appendix B that our calculations reproduce also anomalies in neutron intensities produced by two lower quasiparticles (marked T_1 and L_1 in Fig. 9) in other parts of the BZ (see Fig. 10).

We demonstrate below that all quasiparticles just discussed (i.e., T_1, T_2 and L_1, L_2) are observed also in our ESR experiment in the stripe phase at finite field. Besides, we obtain also low-intensive excitations looking as close satellites of T_1, T_2, and L_1 which are indistinguishable in Fig. 9 and which are not mentioned in this section.

VII. THEORETICAL DESCRIPTION OF ESR RESULTS AT H∥b AND DISCUSSION

We find using the BOT that the ground state of model (3) with parameters (7) obeys the stripe and the UUD spin
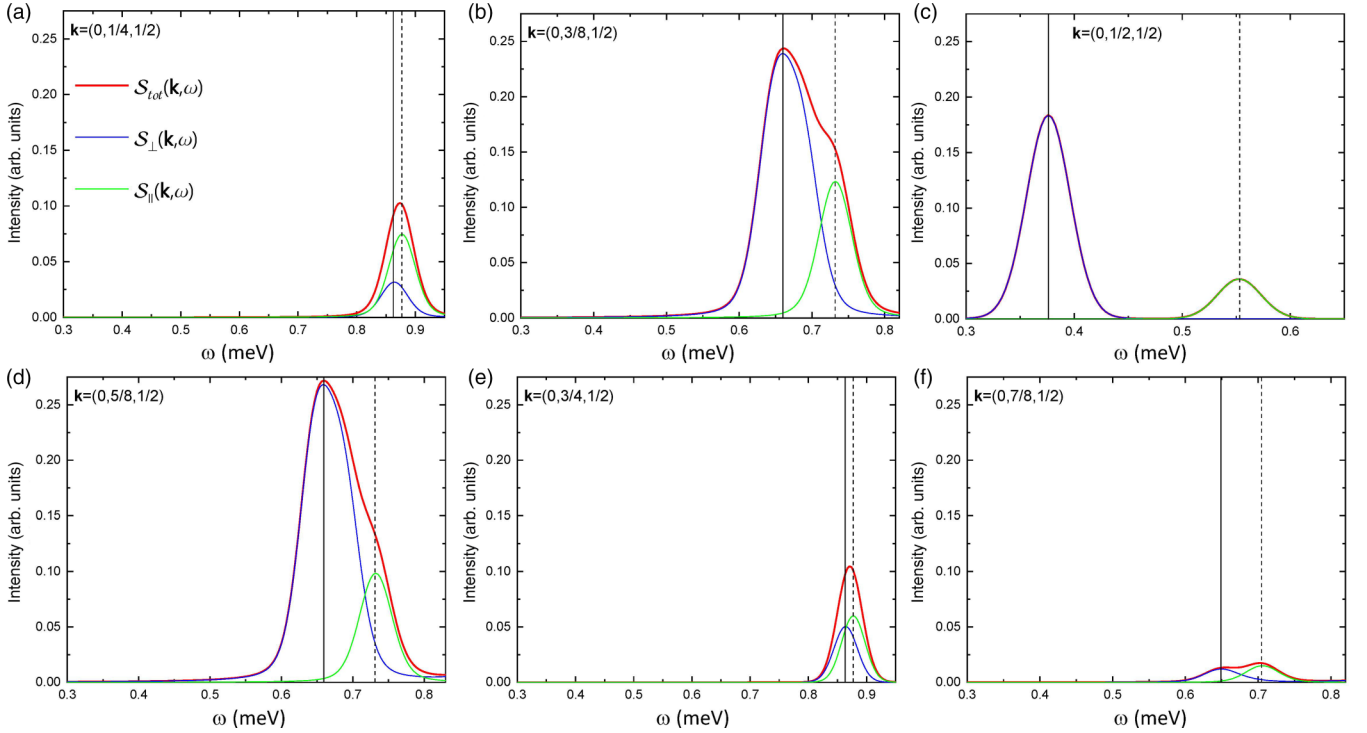
FIG. 10. (a)–(f) Dynamical structure factor (DSF) $\mathcal{S}_{tot}(\mathbf{k}, \omega)$ given by Eq. (B3) and calculated within the BOT to first order in $1/n$ with the plaquette-like unit cell at selected momenta. Contributions to $\mathcal{S}_{tot}(\mathbf{k}, \omega)$ of transverse $\mathcal{S}_{\perp}(\mathbf{k}, \omega)$ and longitudinal $\mathcal{S}_{\parallel}(\mathbf{k}, \omega)$ DSFs are also shown. The neutron cross section is integrated in the interval $(-5, 5)$ of the momentum component perpendicular to triangular planes. Dashed and solid vertical lines mark positions of peaks obtained theoretically in the longitudinal and transverse DSFs, respectively (i.e., energies of well-defined spin-0 and spin-1 excitations denoted as L_1 and T_1 in Fig. 9). Theoretical results are convoluted with the energy resolution of 0.02 meV [inherent to the experimental data presented in Fig. 3(a) of Ref. [12]]. The maxima of $\mathcal{S}_{tot}(\mathbf{k}, \omega)$, the shape of its ω dependence and the integral intensity correspond well to the experimental data in Fig. 3(a) of Ref. [12], where a false color plot is presented of the neutron-scattering intensity.

orderings within experimentally found boundaries of these phases. The longitudinal magnetization is obtained to be equal to zero and $M_s/3$ in these two states, respectively, where M_s is the saturation magnetization [28]. It is difficult to discuss within the BOT transitions to the SDW phase from the stripe and from the UUD states because the SDW has an incommensurate ordering and because these transitions are of the first-order type, as our ESR measurements indicate. We find that the transition from the UUD state to the paramagnet phase takes place near 4 T (in agreement with experiment) as a result of a "condensation" of the lower magnon mode at an incommensurate momentum. The transition from the saturated state (in which all pseudospins are oriented along the field) to the paramagnet one occurs upon "condensation" of spin-2 excitations. However, the spectrum of spin-2 excitations acquires great renormalization to first order in $1/n$ (see Appendix A) within the BOT that makes our technique unsuitable for discussion of this phase transition (one has to go beyond first order in $1/n$, which is a difficult task). Then, we do not consider theoretically in detail phase transitions (and do not determine boundaries of phases) and focus on spectra inside the stripe, the UUD, and the saturated phases within their experimentally determined boundaries.

A. Stripe phase

Both transverse and longitudinal polarizations of microwave field with respect to the external field are present in our ESR experiment because the sample size is comparable to the length of the electromagnetic wave. That is why both spin-0 and spin-1 excitations can appear in our ESR measurements. In addition, spin-0 excitations from the longitudinal channel can arise in our experiment also due to a small anisotropic interaction and/or a small transverse magnetic field component.

We plot in Fig. 5 the theoretical spectra at $\mathbf{k} = \mathbf{0}$ of spin-1 and spin-0 quasiparticles by solid and dashed lines, respectively, which we obtain within the four-spin BOT with the plaquette-like unit cell. Spin-1 modes are denoted T_1, T_2, T_{1s}, T_{2s} and spin-0 excitations are denoted L_1, L_2, L_{1s}. Linewidths in Fig. 5 are proportional to the spectral weights of the corresponding poles in the transverse and in the longitudinal dynamical structure factors $\mathrm{Im}\chi_{\perp}(\mathbf{0}, \omega)$ and $\mathrm{Im}\chi_{\parallel}(\mathbf{0}, \omega)$ [see Eqs. (5) and (6)].

It is seen from Fig. 5 that lines T_1, T_2, and L_1 obtained within the BOT have much less intense satellites T_{1s}, T_{2s}, and L_{1s}. The origin of satellites of two spin-1 excitations can be explained as follows: Notice first that T_1 and T_2 excitations correspond to magnons which appear also within the linear SWT [as in Ref. [11] considering model (3)], where

they are both doubly degenerate due to four spins in the magnetic unit cell. These spin-1 lines are split by quantum fluctuations within the BOT resulting in T_{1s} and T_{2s} satellites. Such modes splitting was observed by the BOT also in other models [26,29] (the splitting of magnon spectrum obtained in Ref. [26] at point M of the BZ in the triangular-lattice Heisenberg model is in agreement with experiment).

Notice that the crystallographic momentum $(0, 1/2, 1/2)$ discussed above in the neutron experiment corresponds to $(0,1,1)$ momentum (which, in turn, is equivalent to $\mathbf{k} = \mathbf{0}$) in the considered BOT with the plaquette-like unit cell. That is why modes T_1, T_2 and L_1, L_2 are the same in Figs. 5 and 9. Weak satellites T_{1s} and T_{2s} predicted by the BOT are too close to the intense T_1, T_2 to be resolved in the neutron experiment at $H = 0$.

It is seen from Figs. 9 and 10 that T_1 and L_1 excitations observed in the BOT describe quite accurately two lower neutron anomalies and modes d and e in the ESR data in Fig. 5. However, the lower strong signal d obtained experimentally has three less intense satellites a, b, and c instead of one T_{1s} predicted by the theory. We have no explanation for this discrepancy at the moment. Extra satellites may be a result of small spin interactions not included in our model. It is also seen from Fig. 5 that weak satellite mode L_{1s} is not detected experimentally.

The upper intense spin-1 mode shown in Fig. 5 corresponds to the T_2 quasiparticle in Fig. 9. As discussed above, the spectrum of this mode is renormalized downward considerably by strong in-chain spin fluctuations which are not taken into account properly to first order in $1/n$ in the version of the BOT with plaquette-like unit cell. At $H = 0$, the downward renormalization arises from 0.84 meV $\approx$ 203 GHz to 0.72 meV $\approx$ 174 GHz (see Fig. 9). A simple shift down of the T_2 curve by the same 30 GHz brings it quite close to the g mode observed in the ESR experiment (see Fig. 5). Then, we relate mode g to T_2.

The upper spin-0 mode in Fig. 5 corresponds to the L_2 elementary excitation in Fig. 9(a) (i.e., to the bound state of two magnons in neighboring chains). It is seen from Fig. 5 that its spectrum is very close below 150 GHz to weak f mode observed experimentally.

It should be noted also that, despite a first-glance chaotic variety of ESR modes, two bright branches d and g going down and up upon the field increasing are similar to the spectrum of a collinear antiferromagnet in magnetic field directed along its easy axis. The falling branch of the conventional antiferromagnet should soften at the spin-flop field. However, the spin-flop transition does not occur in Cs_2CoBr_4 because of the earlier transition to the SDW phase. This results in a finite frequency of mode d at the right boundary of the stripe phase in Fig. 5. In the conventional antiferromagnet with two axes of anisotropy, the rising and falling antiferromagnetic resonance branches have different frequencies at zero field. We observe this difference of d and g modes at $H = 0$ in Cs_2CoBr_4 which have frequencies of 95 and 160 GHz, respectively. SWT [11] and BOT reproduce this splitting which is a result of the chain-alternating easy-plane anisotropy in the model.

To conclude, the multimode ESR spectra of Cs_2CoBr_4 are well described in the stripe phase by model (1) using the BOT. Of the eight observed modes, two bright and three weak

modes are captured by the theory. Only very weak anomalies a, b, and u remain unexplained. We demonstrate that the uniform dynamics (at $\mathbf{k} = \mathbf{0}$) of Cs_2CoBr_4 is not limited to in-chain excitations. The quantitative agreement between our theoretical and experimental findings is not satisfactory above $\approx$150 GHz $\approx$ 0.6 meV (see Figs. 5 and 9) due to pronounced in-chain spin correlations which cannot be properly taken into account within the first order in $1/n$ of the BOT (see also Sec. VI).

B. UUD phase

We consider elementary excitations in the UUD phase within the three-spin variant of the BOT as in Ref. [27], where triangular-lattice Heisenberg antiferromagnet in magnetic field was discussed. The results obtained are depicted in Fig. 5. It is seen that the theoretically found T_3 quasiparticle carrying spin 1 describes well the brightest lower mode l while we do not observe theoretically its three low-intensity satellites (k, m, and n modes). The splitting of l mode and the appearance of satellites might be again due to small spin interactions not taken into account [for instance, small interplane interaction is known to produce a mode splitting in triangular-lattice antiferromagnet $RbFe(MoO_4)_2$ [30]]. The spectrum of the lower spin-0 excitation L_3 obtained in the BOT does not practically depend on H so that it is very difficult to observe it using the ESR technique. Such spin-0 quasiparticles lying below magnon modes were found also in Ref. [27] in the UUD state of the triangular-lattice Heisenberg antiferromagnet.

The mode o obtained experimentally and shown in Fig. 5 is described well (with 15% accuracy) by the T_4 excitation found theoretically. Similar to the stripe phase, there is no good quantitative agreement between our theoretical and experimental findings above $\approx$150 GHz (see Fig. 5).

Notice that the observed field behavior of the low-lying spin-1 modes l and o (T_3 and T_4) reproduces qualitatively the field evolution of two lower magnons in the triangular-lattice Heisenberg antiferromagnet in the UUD phase [21]: one branch falls to zero at the right boundary of the UUD phase while another branch rises monotonically from the left limit of the UUD range.

C. Saturated phase

The saturated phase in which all pseudospins are oriented along the magnetic field has been considered using the four-spin variant of the BOT with the plaquette-like unit cell. It is seen from Fig. 5 that spectra of lower spin-1 quasiparticles (denoted T_6 and T_7) describe reasonably well the w and p modes observed experimentally. We obtain also a high-energy bright spin-1 excitation (corresponding to the experimentally found mode s in Fig. 5) and much weaker spin-2 quasiparticles around it which correspond presumably to experimentally found modes t and q in Fig. 5. However, our theory overestimates the energies of the s, t, and q modes by more than 40% (so that we do not show the corresponding theoretical lines in Fig. 5). We attribute this discrepancy, in particular, to the need to take into account the omitted $|\pm 3/2\rangle$ one-ion states which come into play at energies $\gtrsim$250 GHz.

Interestingly, there is also another low-lying spin-2 excitation (which can appear in common methods as a two-magnon bound state) whose energy, however, is renormalized downward considerably by the first $1/n$ corrections. This is an indication that one needs to go beyond the first order in $1/n$ to obtain this spectrum accurately (that is out of the scope of the present work). We do not show the spectrum of this spin-2 quasiparticle in Fig. 5.

D. Spin-density wave and paramagnet phase

The theoretical interpretation of ESR data in the SDW and in the paramagnet phases is out of the scope of the present paper.

VIII. SUMMARY AND CONCLUSION

To summarize, we discuss the ground-state spin dynamics of strongly anisotropic distorted-triangular-lattice antiferromagnet Cs_2CoBr_4 by ESR measurements up to 250 GHz and present a theoretical analysis. In this compound, the interplay of frustration, quantum fluctuations, low dimensionality, and strong anisotropy gives rise to at least six phases in different orientations of magnetic field $\mathbf{H}$ [10,11]. Among them are states which are characteristic to 3D antiferromagnets (collinear stripe state), quasi-1D magnets [collinear incommensurate spin-density-wave (SDW) phase], and triangular-lattice antiferromagnets [up-up-down (UUD) state with 1/3-magnetization plateau]. We observe by the ESR a rich zoo of excitations in phases arising in $\mathbf{H}$ directed along and perpendicular to the magnetic easy axis b which are collected in Figs. 5 and 8.

Due to strong single-ion anisotropy in spin-$\frac{3}{2}$ Co^{2+} ions, the low-energy spin dynamics of Cs_2CoBr_4 which is modeled by Hamiltonian (1) can be described by a strongly anisotropic pseudospin-$\frac{1}{2}$ Hamiltonian (3) [10,11]. Owing to spatial anisotropy of exchange couplings, models (1) and (3) can be also viewed as spin chains passing along the b axis. There are two types of chains in which easy-plane anisotropies are almost perpendicular to each other and they intersect along the b axis (see Fig. 1). This makes the b axis the easy direction of the whole system. We consider model (3) theoretically using the bond operator technique (BOT) described in some detail in Appendix A and which is similar in spirit to the well-known spin-wave theory (SWT). However the BOT is more convenient in discussion of "complex" excitations which appear in other approaches as bound states of ordinary quasiparticles (magnons or triplons) [22,26,27,29,31].

In the low-field collinear two-sublattice stripe state at $\mathbf{H}\|b$, the number of modes which we observe using the ESR exceeds essentially the set of magnetic resonance modes of a conventional antiferromagnet (see Fig. 5). However, many of these excitations are described using the BOT with model parameters (7). Spectra of spin-1 (magnons) and spin-0 (two-magnon bound states) quasiparticles obtained theoretically are also shown in Fig. 5. We demonstrate that the d and g ESR signals are described by spin-1 quasiparticles denoted in Fig. 5 as T_1 and T_2, which are the conventional magnons expected in a two-axis quasi-2D magnet strongly renormalized by quantum fluctuations. In the semiclassical SWT, each of T_1 and

T_2 are doubly degenerate due to four different spins in the magnetic unit cell (see Fig. 1). However quantum fluctuations taken into account more accurately within the BOT lift this degeneracy and produce bright lines T_1 and T_2 with weak satellites T_{1s} and T_{2s}. The latter is not detected in experiment presumably due to its weakness while the brightest mode d has three satellites a, b, and c instead of one T_{1s}. The increasing number of satellites may be related to small spin interactions which are not included in the model and which frequently lead to modes splitting in other systems (interplane interaction, dipolar forces, etc.). Spin-0 excitations L_1 and L_2 in Fig. 5 are bound states of two magnons propagating inside the same and in neighboring spin chains, respectively. It is seen from Fig. 5 that their spectra follow ESR modes e and f. The weak satellite L_{1s} predicted by the theory is not detected experimentally. Thus, the modes T_1, T_2, T_{1s}, L_1, L_2 carrying the most of the spectral weight are attributed to the observed modes. Only very weak satellites are not captured by the theory, they may arise, e.g., due to the weak interaction between magnetic layers.

It is seen from Fig. 5 that the agreement between the theory and experiment becomes worse above 150 GHz. Using two unit cells in the BOT differing in their geometry, we argue that this discrepancy is due to profound 1D spin fluctuations inside spin chains which cannot be taken into account properly to first order in $1/n$ of the BOT. The confirmation of this comes also from previous neutron-scattering and terahertz spectroscopy experiments [12] in which up to nine sharp anomalies were observed at the BZ zone center which resemble a Zeeman ladder (ZL) in Ising-like spin chains. These anomalies were related to bound states of two domain walls inside individual chain confined by interplane interaction [12]. Energies of all these anomalies were described by negative roots of the Airy function (as it is done in conventional ZLs [14–20]) except for three lower ones [12]. We show in Figs. 9 and 10 that two low-energy peaks are reproduced quantitatively within the BOT in model (3) in which the interplane interaction is ignored. Besides, these anomalies correspond to spin-1 and spin-0 quasiparticles T_1 and L_1 which cannot be parts of the same ZL. Last but not least, the field evolution of modes d, e, f, and g shown in Fig. 5 has nothing to do with field behavior of levels in spin-0 and/or spin-1 ZLs (see, e.g., Refs. [18,19] and Sec. I).

Taking into account, however, the successful description in Ref. [12] of levels lying above 200 GHz (0.8 meV) within the ZL formalism and bearing in mind our own results described above, we can state that Cs_2CoBr_4 combines features in its spin dynamics characteristic of both 2D and 1D anisotropic systems at energies smaller and larger than 0.8 meV, respectively.

In the UUD state of Cs_2CoBr_4, similar to the UUD phase in the Heisenberg triangular-lattice antiferromagnet [27], we observe theoretically two magnon branches denoted in Fig. 5 as T_4 and T_5 which go up upon the field increasing and magnon T_3 whose energy falls down. Besides, two spin-0 quasiparticles L_3 and L_4 are detected one of which lies below magnons that is also in a qualitative agreement with the Heisenberg model [27]. It is seen from Fig. 5 that the brightest ESR modes l and o follow spectra of T_3 and T_4 magnons. As in the stripe phase, we notice that the most intensive mode l has three weak

satellites k, m, and n whose origin is not clear now and that the agreement between the theory and experiment becomes worse upon increasing the energy. The low-intensive spin-0 modes are not detected experimentally (in the case of L_3, this may be related also to its weak-field dependence).

In the saturated state, three high-energy ESR modes can be described only qualitatively using the BOT. We identify the most intensive mode s as a spin-1 excitation which is surrounded by two spin-2 quasiparticles t and q (corresponding theoretical curves are not shown in Fig. 5). Lower ESR signals p and w are described reasonably good by two spin-1 excitations marked in Fig. 5 as T_6 and T_7.

We leave for the future the theoretical description of two lines of ESR signals in the SDW (Fig. 5), numerous modes observed in the paramagnet phases (Fig. 5), and spin dynamics at **H**∥c (Fig. 8).

ACKNOWLEDGMENTS

APPENDIX A: BOND OPERATOR TECHNIQUE FOR SPIN-$\frac{1}{2}$ MODELS

The main idea of the bond operator technique (BOT) is to take into account all spin degrees of freedom in the magnetic unit cell containing several spins 1/2 by building a bosonic spin representation reproducing the spin commutation algebra. A general scheme of construction of such a representation for arbitrary numbers of spins in the unit cell is described in detail in Ref. [22]. We consider now briefly the main steps of this procedure by the example of four spins in the unit cell, which is relevant for the stripe phase in model (3). First, we introduce 15 Bose operators in each unit cell which act on 16 basis functions of four spins $|0\rangle$ and $|e_i\rangle$ ($i = 1, \ldots, 15$) according to the rule

$$a_i^\dagger |0\rangle = |e_i\rangle, \quad i = 1, \ldots, 15, \quad \text{(A1)}$$

where $|0\rangle$ is a selected state playing the role of the vacuum. Then, we build the bosonic spin transformation in the unit cell as it is described in Ref. [22] which turns out to be quite bulky and which is presented in Ref. [22]. The code in the *Mathematica* software which generates this representation is also available in Ref. [32]. There is a formal artificial parameter n in this spin transformation that appears in operator $(n - \sum_{i=1}^{15} a_i^\dagger a_i)^{1/2}$ by which linear in Bose operators terms are multiplied [cf. the term $(2S - a^\dagger a)^{1/2}$ in the Holstein-Primakoff representation]. It prevents mixing of states containing more than n bosons and states with no more than n bosons (then, the physical results of the BOT correspond to $n = 1$). Besides, all constant terms in our spin transformation are proportional to n whereas bilinear in Bose operators terms do not depend on n and have the form $a_i^\dagger a_j$.
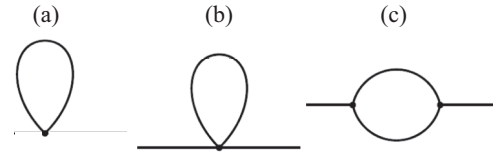

FIG. 11. Diagrams giving corrections to first-order in $1/n$ to (a) the ground-state energy and the staggered magnetization, and (b), (c) to the self-energy parts.

We introduce also separate representations via operators (A1) for terms $\mathbf{s}_i\mathbf{s}_j$, $s_i^x s_j^x$, $s_i^y s_j^y$, and $s_i^z s_j^z$ in the Hamiltonian in which i and j belong to the same unit cell. Constant terms in these representations are proportional to n^2 and terms of the form $a_i^\dagger a_j$ are proportional to n [22]. Thus, we obtain a close analog of the conventional Holstein-Primakoff spin transformation which reproduces the commutation algebra of all spin operators in the unit cell for all $n > 0$ and in which n is the counterpart of the spin value S. In analogy with the spin-wave theory (SWT), expressions for observables are found in the BOT using the conventional diagrammatic technique as series in $1/n$. This is because terms in the Bose-analog of the spin Hamiltonian containing products of i Bose operators are proportional to $n^{2-i/2}$ (in the SWT, such terms are proportional to $S^{2-i/2}$). For instance, to find the ground-state energy, the staggered magnetization and self-energy parts to first order in $1/n$, one has to calculate diagrams shown in Fig. 11 (as in the SWT to first order in $1/S$).

Notice that states $|0\rangle$ and $|e_i\rangle$ in Eq. (A1) are linear combinations of elementary quantum states which are simple products of states $|\uparrow\rangle$ and $|\downarrow\rangle$ of each spin in the unit cell. Coefficients in these combinations contain parameters which should be found by minimizing the term in the Hamiltonian not containing Bose operators (linear in Bose operator terms in the Hamiltonian vanish at this set of parameters) [22]. In particular, we determine in this way properties of the ground state (e.g., the spin ordering) to zeroth order in $1/n$.

Previous applications of the BOT to two-dimensional spin-$\frac{1}{2}$ systems well studied before both theoretically (by other numerical and analytical methods) and experimentally show that the first $1/n$ terms in most cases give the main corrections to renormalization of observables if the system is not very close to a quantum critical point [22,26,27,29,31,33]. Similarly, the first $1/S$ corrections in the SWT frequently make the main quantum renormalization of observable quantities even at $S = 1/2$, see, e.g., Ref. [34]. Importantly, because the spin commutation algebra is reproduced in our method at any $n > 0$, the proper number of Goldstone excitations arises in ordered phases to any order in $1/n$ (unlike the vast majority of other versions of the BOT proposed so far [22]).

As quantum spin correlations inside the unit cell are taken into account accurately within the BOT, we achieved a quite precise description of salient features of short-wavelength quasiparticles in different systems some of which cannot be described even qualitatively using conventional analytical approaches [26,27,29,31]. Although the BOT is technically very similar to the SWT, the main disadvantage of this technique is that it is very bulky (e.g., the part of the Hamiltonian

bilinear in Bose operators contains more than 100 terms) and it requires time-consuming numerical calculation of diagrams.

The three-spin variant of the BOT can be constructed in a similar way. It was used in Refs. [26,27,29] for consideration of various ordered phases in triangular-lattice antiferromagnets. The code in the *Mathematica* software which generates this spin transformation can be found in Ref. [35]. We employ in this study the three-spin variant of the BOT for discussion of the UUD state and the four-spin variant is utilized for consideration of the stripe and the saturated phases.

Notice that the BOT allows us to consider numerous complex excitations which can arise in standard approaches as bound states of conventional quasiparticles (magnons or triplons) [22]. For instance, there are only four bosons in the four-spin BOT which describe conventional magnons in the stripe phase. The remaining 11 bosons are responsible for some other excitations which are built on quantum states of the whole unit cell [see Eq. (A1)]. In common methods, discussion of the bound states requires analysis of some infinite series of diagrams for vertexes. As a result, spectra of bound states cannot be obtained as series of some parameter within conventional approaches because it is normally impossible to take into account all the required diagrams. In contrast, the existence of separate bosons in BOTs (describing some bound states in considered models) allows us to find their spectra as series in $1/n$ by calculating the same diagrams as for the common quasiparticles [e.g., diagrams shown in Figs. 11(b) and 11(c) in the first order in $1/n$]. For instance, in the ordered phase of the isotropic square-lattice antiferromagnet, the version of the BOT with a two-site unit cell contains three bosons describing two spin-1 excitations (conventional magnons) and one spin-0 quasiparticle (the Higgs mode) [22]. The price to pay for increasing the quasiparticles zoo is the bulky theory.

In the present study, we discuss the stripe phase at zero field [model (B2)] using four-spin BOT with two variants of the unit cell: the plaquette-like unit cell containing two couples of spins from neighboring chains and the chain-like unit cell with four spins from the same chain (see insets in Fig. 9). This allows us to reveal the role of 1D correlations in the considered model on conventional spin-1 excitations (magnons) and on spin-0 quasiparticles (which could arise in the SWT as bound states of two magnons) appearing in the longitudinal channel.

We take into account diagrams shown in Figs. 11(b) and 11(c) to find all self-energy parts $\Sigma(\omega, \mathbf{k})$ in the first order in $1/n$. We use (bare) Green's functions of the harmonic approximation in these calculations. Spectra of elementary excitations are obtained by finding zeros of Green's function denominators taking into account the ω dependence of self-energy parts. This scheme of calculations proved to give an accurate description of elementary excitations some of which had no counterparts not only in the semiclassical spin-wave theory but also in the harmonic approximation of the BOT [26,27,29,31].

APPENDIX B: NEUTRON-SCATTERING CROSS-SECTION CALCULATION

We provide in this Appendix some technical details of the neutron-scattering cross-section calculation at $H = 0$.

At zero field, model (3) can be simplified further by performing the canonical transformation

$$s_{2i,j}^x = -\tilde{s}_{2i,j}^y, \quad s_{2i,j}^y = -\tilde{s}_{2i,j}^x, \quad s_{2i,j}^z = -\tilde{s}_{2i,j}^z \quad \text{(B1)}$$

which is a result of subsequent rotations by $\pi/2$ around z axis and by π around y axis in chains with even numbers. After this transformation, all chains become equivalent and the Hamiltonian acquires the form

$$
\begin{aligned}
\mathcal{H}_{ps}^{H=0} = \sum_{i,j} \Big[& 4J\big(\tilde{\mathbf{s}}_{i,j}\tilde{\mathbf{s}}_{i,j+1}\big) - 3J\tilde{s}_{i,j}^y\tilde{s}_{i,j+1}^y \\
& + 4A_1\tilde{s}_{i,j}^z\tilde{s}_{i,j+1}^z - 2J'\big(\tilde{s}_{i,j}^x\tilde{s}_{i+1,j}^y + \tilde{s}_{i,j}^y\tilde{s}_{i+1,j}^x\big) \\
& - 2J'\big(\tilde{s}_{i,j}^x\tilde{s}_{i+1,j-1}^y + \tilde{s}_{i,j}^y\tilde{s}_{i+1,j-1}^x\big) \\
& - 4(J' - A_2)\big(\tilde{s}_{i,j}^z\tilde{s}_{i+1,j}^z + \tilde{s}_{i,j}^z\tilde{s}_{i+1,j-1}^z\big)\Big].
\end{aligned}
\quad \text{(B2)}
$$

Notice that there is no such canonical transformation making chains equivalent at finite field.

The chains equivalence in Eq. (B2) allows us to apply two modifications of the four-spin BOT with two kinds of the unit cell to reveal the character of low-energy excitations observed recently in neutron experiment [12] and in our ESR measurements.

To describe available neutron data, we calculate the following dynamical structure factor [25]:

$$\mathcal{S}(\mathbf{k}, \omega) = \frac{1}{\pi}\text{Im}\sum_{\alpha,\beta} g_\alpha g_\beta(\delta_{\alpha\beta} - \widehat{k}_\alpha\widehat{k}_\beta)\chi_{\alpha\beta}(\mathbf{k}, \omega), \quad \text{(B3)}$$

where $\alpha, \beta = x, y, z$, $\widehat{\mathbf{k}} = \mathbf{k}/k$, $\chi_{\alpha\beta}(\mathbf{k}, \omega)$ are given by Eq. (4), and we use that the g tensor is diagonal and has components $g_x = 2.37(1)$, $g_y = 2.42(1)$, and $g_z = 2.47(2)$ [10]. For the plaquette-like and the chain-like unit cells shown in insets of Fig. 9, $\mathbf{S_k}$ in Eq. (4) has the form

$$\mathbf{S_k} = \tfrac{1}{2}(\mathbf{S}_{1\mathbf{k}} + \mathbf{S}_{2\mathbf{k}}e^{-ik_2/2} + \mathbf{S}_{3\mathbf{k}}e^{-i(k_1+k_2)/2} + \mathbf{S}_{4\mathbf{k}}e^{-ik_1/2}),$$
(B4)

and

$$\mathbf{S_k} = \tfrac{1}{2}(\mathbf{S}_{1\mathbf{k}} + \mathbf{S}_{2\mathbf{k}}e^{-ik_1/4} + \mathbf{S}_{3\mathbf{k}}e^{-ik_1/2} + \mathbf{S}_{4\mathbf{k}}e^{-i3k_1/4}), \quad \text{(B5)}$$

where $\mathbf{k} = k_1\mathbf{f}_1 + k_2\mathbf{f}_2$, $\mathbf{f}_{1,2}$ are reciprocal-lattice vectors corresponding to translation vectors $\mathbf{u}_1$ and $\mathbf{u}_2$ in the real space depicted in the insets of Fig. 9, and $\mathbf{S}_i$ is the ith spin operator in the unit cell which is related with pseudospin $\tilde{\mathbf{s}}_i$ via Eqs. (2) and (B1).

Figure 10 shows two lower anomalies (labeled in Fig. 9 as T_1 and L_1) in neutron-scattering intensity $\mathcal{S}_{\text{tot}}(\mathbf{k}, \omega)$ given by Eq. (B3) and calculated within the BOT in the first order in $1/n$ with the plaquette-like unit cell for six momenta. There is a good agreement of Fig. 10 with neutron data presented in Fig. 3(a) of Ref. [12] in energies, shapes, and magnitudes of two lower maxima.

[1] L. Balents, Spin liquids in frustrated magnets, Nature (London) **464**, 199 (2010).

[2] O. A. Starykh, Unusual ordered phases of highly frustrated magnets: a review, Rep. Prog. Phys. **78**, 052502 (2015).

[3] A. Kitaev, Anyons in an exactly solved model and beyond, Ann. Phys. (NY) **321**, 2 (2006).

[4] S. A. Zvyagin, A. N. Ponomaryov, J. Wosnitza, D. Hirai, Z. Hiroi, M. Gen, Y. Kohama, A. Matsuo, Y. H. Matsuda, and K. Kindo, Dimensional reduction and incommensurate dynamic correlations in the $S = 1/2$ triangular-lattice antiferromagnet $Ca_3ReO_5Cl_2$, Nat. Commun. **13**, 6310 (2022).

[5] M. Kohno, O. A. Starykh, and L. Balents, Spinons and triplons in spatially anisotropic frustrated antiferromagnets, Nat. Phys. **3**, 790 (2007).

[6] R. Coldea, D. A. Tennant, and Z. Tylczynski, Extended scattering continua characteristic of spin fractionalization in the two-dimensional frustrated quantum magnet Cs_2CuCl_4 observed by neutron scattering, Phys. Rev. B **68**, 134424 (2003).

[7] A. I. Smirnov, K. Y. Povarov, S. V. Petrov, and A. Y. Shapiro, Magnetic resonance in the ordered phases of the two-dimensional frustrated quantum magnet Cs_2CuCl_4, Phys. Rev. B **85**, 184423 (2012).

[8] M. Y. Veillette, A. J. A. James, and F. H. L. Essler, Spin dynamics of the quasi-two-dimensional spin-$\frac{1}{2}$ quantum magnet Cs_2CuCl_4, Phys. Rev. B **72**, 134429 (2005).

[9] D. Heidarian, S. Sorella, and F. Becca, Spin-$\frac{1}{2}$ Heisenberg model on the anisotropic triangular lattice: From magnetism to a one-dimensional spin liquid, Phys. Rev. B **80**, 012404 (2009).

[10] K. Y. Povarov, L. Facheris, S. Velja, D. Blosser, Z. Yan, S. Gvasaliya, and A. Zheludev, Magnetization plateaux cascade in the frustrated quantum antiferromagnet Cs_2CoBr_4, Phys. Rev. Res. **2**, 043384 (2020).

[11] L. Facheris, K. Y. Povarov, S. D. Nabi, D. G. Mazzone, J. Lass, B. Roessli, E. Ressouche, Z. Yan, S. Gvasaliya, and A. Zheludev, Spin density wave versus fractional magnetization plateau in a triangular antiferromagnet, Phys. Rev. Lett. **129**, 087201 (2022).

[12] L. Facheris, S. D. Nabi, A. Glezer Moshe, U. Nagel, T. Rõõm, K. Y. Povarov, J. R. Stewart, Z. Yan, and A. Zheludev, Confinement of fractional excitations in a triangular lattice antiferromagnet, Phys. Rev. Lett. **130**, 256702 (2023).

[13] H. Shiba, Quantization of magnetic excitation continuum due to interchain coupling in nearly one-dimensional Ising-like antiferromagnets, Prog. Theor. Phys. **64**, 466 (1980).

[14] B. M. McCoy and T. T. Wu, Two-dimensional Ising field theory in a magnetic field: Breakup of the cut in the two-point function, Phys. Rev. D: Part. Fields **18**, 1259 (1978).

[15] S. B. Rutkevich, Energy spectrum of bound-spinons in the quantum Ising spin-chain ferromagnet, J. Stat. Phys. **131**, 917 (2008).

[16] R. Coldea, D. A. Tennant, E. M. Wheeler, E. Wawrzynska, D. Prabhakaran, M. Telling, K. Habicht, P. Smeibidl, and K. Kiefer, Quantum criticality in an Ising chain: Experimental evidence for emergent E_8 symmetry, Science **327**, 177 (2010).

[17] B. Grenier, S. Petit, V. Simonet, E. Canévet, L.-P. Regnault, S. Raymond, B. Canals, C. Berthier, and P. Lejay, Longitudinal and transverse Zeeman ladders in the Ising-like chain antiferromagnet $BaCo_2V_2O_8$, Phys. Rev. Lett. **114**, 017201 (2015).

[18] S. Kimura, H. Yashiro, K. Okunishi, M. Hagiwara, Z. He, K. Kindo, T. Taniyama, and M. Itoh, Field-induced order-disorder transition in antiferromagnetic $BaCo_2V_2O_8$ driven by a softening of spinon excitation, Phys. Rev. Lett. **99**, 087602 (2007).

[19] Z. Wang, J. Wu, S. Xu, W. Yang, C. Wu, A. K. Bera, A. T. M. N. Islam, B. Lake, D. Kamenskyi, P. Gogoi, H. Engelkamp, N. Wang, J. Deisenhofer, and A. Loidl, From confined spinons to emergent fermions: Observation of elementary magnetic excitations in a transverse-field Ising chain, Phys. Rev. B **94**, 125130 (2016).

[20] A. K. Bera, B. Lake, F. H. L. Essler, L. Vanderstraeten, C. Hubig, U. Schollwöck, A. T. M. N. Islam, A. Schneidewind, and D. L. Quintero-Castro, Spinon confinement in a quasi-one-dimensional anisotropic Heisenberg magnet, Phys. Rev. B **96**, 054423 (2017).

[21] A. V. Chubukov and D. I. Golosov, Quantum theory of an antiferromagnet on a triangular lattice in a magnetic field, J. Phys.: Condens. Matter **3**, 69 (1991).

[22] A. V. Syromyatnikov, Collective excitations in spin-$\frac{1}{2}$ magnets through bond-operator formalism designed both for paramagnetic and ordered phases, Phys. Rev. B **98**, 184421 (2018).

[23] A. I. Smirnov, T. A. Soldatov, and V. S. Edelman, Dilution microcryostat insert for microwave spectroscopy and magnetic resonance, Instrum. Exp. Tech. **65**, 668 (2022).

[24] T. A. Soldatov, A. I. Smirnov, and A. V. Syromyatnikov, following paper, Dynamics of anisotropic frustrated antiferromagnet Cs_2CoBr_4 in a spin-liquid regime, Phys. Rev. B **108**, 184427 (2023).

[25] S. W. Lowesey, *Theory of Neutron Scattering by Condensed Matter* (Oxford University Press, Oxford, 1987).

[26] A. V. Syromyatnikov, Elementary excitations in spin-$\frac{1}{2}$ antiferromagnets on the triangular lattice, Phys. Rev. B **105**, 144414 (2022).

[27] A. Syromyatnikov, Unusual dynamics of spin-$\frac{1}{2}$ antiferromagnets on the triangular lattice in magnetic field, Ann. Phys. (NY) **454**, 169342 (2023).

[28] To be precise, the longitudinal magnetization per spin increases upon the field increasing from 0 to 0.006 in the stripe phase and by 0.7% in the UUD state.

[29] A. V. Syromyatnikov, Dynamics of spin-$\frac{1}{2}$ J_1–J_2 model on the triangular lattice, Phys. Rev. B **106**, 184415 (2022).

[30] L. E. Svistov, A. I. Smirnov, L. A. Prozorova, O. A. Petrenko, L. N. Demianets, and A. Y. Shapiro, Quasi-two-dimensional antiferromagnet on a triangular lattice $RbFe(MoO_4)_2$, Phys. Rev. B **67**, 094434 (2003).

[31] A. V. Syromyatnikov, Multiple magnon modes in spin-$\frac{1}{2}$ Heisenberg antiferromagnet on simple square lattice in strong magnetic field, Phys. Rev. B **102**, 014409 (2020).

[32] A. V. Syromyatnikov (2022) See Supplemental Material at http://link.aps.org/supplemental/10.1103/PhysRevB.106.184415 for the code in the *Mathematica* software which generates the spin representation which we use in the present work for consideration of the stripe phase.

[33] A. V. Syromyatnikov and A. Y. Aktersky, Elementary excitations in the ordered phase of spin-$\frac{1}{2}$ J_1–J_2 model on square lattice, Phys. Rev. B **99**, 224402 (2019).

[34] E. Manousakis, The spin- 1/2 Heisenberg antiferromagnet on a square lattice and its application to the cuprous oxides, Rev. Mod. Phys. **63**, 1 (1991).

[35] A. V. Syromyatnikov (2022) See Supplemental Material at http://link.aps.org/supplemental/10.1103/PhysRevB.106.184415 for the code in the Mathematica software which generates the spin representation which we use in the present work for consideration of the "up-up-down" phase.